Superior Catalytic Performance of Atomically Dispersed Palladium on Graphene in CO Oxidation

Xin Liu, Meng Xu, Lingyun Wan, Hongdan Zhu, Ke Xin Yao, Roberto Linguerri, Gilberte Chambaud, Yu Han, Changgong Meng

ACS Catalysis

pubs.acs.org/acscatalysis

Research Article

Superior Catalytic Performance of Atomically Dispersed Palladium on Graphene in CO Oxidation

Xin Liu,* Meng Xu, Lingyun Wan, Hongdan Zhu, Kexin Yao, Roberto Linguerri, Gilberte Chambaud, Yu Han,* and Changgong Meng*

Cite This: *ACS Catal.* 2020, 10, 3084−3093

Read Online

ACCESS | Metrics & More | Article Recommendations | Supporting Information

ABSTRACT: Although substantial advances have been made in a few reactions of industrial significance over single-atom catalysts (SACs), the origin of the superior catalytic performance, the nature of the active sites, and the reaction pathways are still the subject of debate. Even for CO oxidation over SACs on nonreducible substrates, the understanding is limited. We investigated the performance of Pd atoms monodispersed on graphene (PdGr) in CO oxidation. Combining first-principles-based thermodynamics calculations and microkinetics modeling, we showed that the positively charged PdGr can exhibit a rather high low-temperature activity in CO oxidation. Under reaction conditions, the Pd atom binds strongly with O_2, acting as the reactive species to convert CO. A comparison of the conversion rates of steps along different potential reaction pathways provides direct evidence that CO oxidation mainly proceeds through revised Langmuir−Hinshelwood pathways, and the dissociation of the peroxide intermediate (O−O−C═O) is the rate-limiting step. The predicted catalytic performance was attributed to the specific electronic structure of PdGr with the positively charged Pd on graphene monovacancy exposing sp-type frontier states. We expect these findings to help in understanding the performance of SACs and to guide the design and fabrication of SACs with superior catalytic performance.

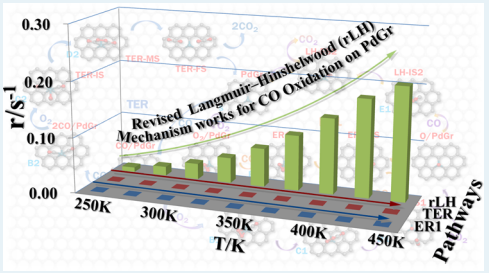

KEYWORDS: *single-atom catalysis, CO oxidation, Langmuir−Hinshelwood, microkinetics modeling, first-principles*

1. INTRODUCTION

Low-temperature catalytic conversion of carbon monoxide (CO) to carbon dioxide (CO_2) via oxidation is one of the key parts of several chemical processes of industrial significance, including CO removal by preferential oxidation in H_2-rich stream for fuel cell applications,[1−4] control of toxic contents in the exhaust gas from combustion engines and automobiles,[5,6] and so forth. Though noble-metal catalysts, including Pt,[7−15] Pd,[16−23] Rh,[24,25] Au,[26−29] Ir,[30,31] and so forth, are highly active in CO oxidation, they are expensive, and their performances are strongly dependent on the reaction conditions.[9,12,32] Considerable attention has been devoted to develop novel CO oxidation catalysts efficient at low temperatures.[31,33,34] For a more profitable use of noble metals, fabrication and application of noble metal-based single-atom catalysts (SACs) have become a new area of focus in the field of catalysis.[29,35−37] Since its rise to prominence, graphene was proposed as a catalyst support because of its large surface area, superior mechanical and chemical properties, and so forth.[38−40] Recently, various graphene-derived SACs have been fabricated[41,42] and proved to be efficient for electrocatalysis,[43−45] olefin hydrogenation and dehydrogenation,[46−52] arene oxidation,[53−55] and CO oxidation.[56−59]

Though substantial advances have been made in a few reactions of industrial significance over SACs, the origin of the superior catalytic performance, the nature of the active sites, and the reaction pathways are still under hot debate. Such concerns exist, especially in the field of SACs over nonreducible supports, such as Al_2O_3, graphene, and graphene-like two-dimensional (2D) materials. Several mechanisms have been proposed for CO oxidation over supported SACs. On SACs over a reducible oxide support, CO oxidation may proceed through a Mars−van-Krevelen pathway, where CO is first oxidized by the O atom of the support and then the reduced support is reoxidized by O_2.[34] Alternatively, the nonreducible supports of certain SACs were proposed to promote the adsorption of reaction species, facilitating the CO oxidation at the metal−support interface.[23,30] As graphene is inert to both CO and O_2, the reaction pathways of this kind are also not applicable to graphene-based SACs.[23,34] Apart from these, because of lack of binding sites for CO, O_2, and O atoms from O_2 activation, the conventional Langmuir−Hinshelwood (LH) and Eley−Rideal (ER) pathways would both be less effective.[60−62] Iglesia et al. investigated CO oxidation over well-defined Pt nanoparticles, and they suggested that the CO oxidation may proceed through a revised LH (rLH) type of

Received: November 8, 2019
Revised: February 4, 2020
Published: February 4, 2020

https://dx.doi.org/10.1021/acscatal.9b04840
ACS Catal. 2020, 10, 3084−3093

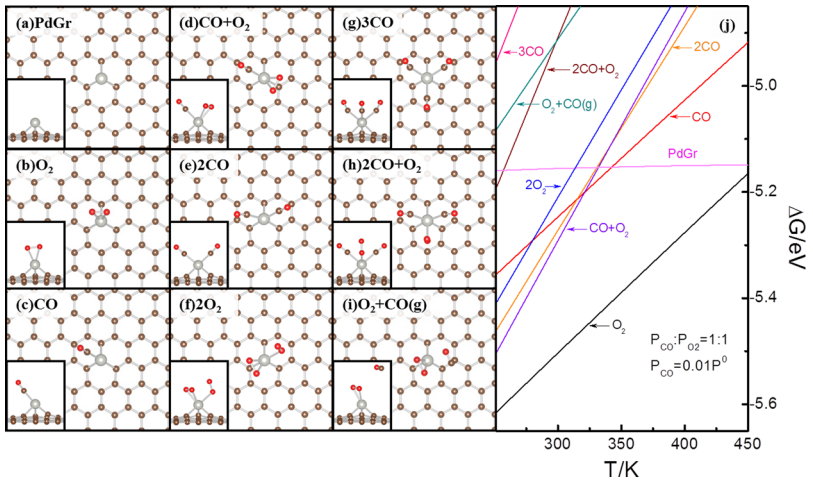

Figure 1. Top (left panel) and side (insets in the left panel) views of the calculated atomic structures and temperature dependence of the Gibbs free energies (ΔG, right panel) for the potential reaction species formed over PdGr in CO oxidation. ΔG was calculated with respect to monovacancy graphene and Pd atom at P_{CO} = 0.01 atm and P_{CO}/P_{O_2} = 1:1.

pathway with a CO-assisted O_2 dissociation, leading to a peroxide species that decomposes to form CO_2 and chemisorbed O.[63] Feng et al. proposed that this is the pathway for CO oxidation over Au_1/graphene SAC.[56] On the other hand, Landman et al. suggested that the carbonate species (CO_3) would be dominant because its formation is more plausible than other alternatives, and this was assumed by Allard et al., Narula et al., and Moses-DeBusk et al. in their investigations on CO oxidation over Pd/Al_2O_3 and Pt/Al_2O_3 SACs.[21,23,64] However, the potential formation of the peroxide species still could not be ruled out.[21] The recent in situ investigation on CO oxidation over Pt/Al_2O_3 SACs by Newton et al. ascribed the observed superior catalytic performance to the "CO_3" species at high frequencies (~1690 cm^{-1}).[12] These findings highlight the superior CO catalytic performance of Pd- and Pt-based SACs, but the detailed reaction pathways still remain a mystery in the absence of understanding the mechanism.

Apart from the rLH mechanism explored by Iglesia et al.[63] and Feng et al.[56], several alternative pathways were also proposed theoretically for CO oxidation over 2D SACs. Chen et al. proposed that over Fe_1/graphene, the approaching CO may facilitate O_2 dissociation by forming CO_3 species and that the reaction would proceed through an ER-type pathway (ER2), with the CO_3 dissociation as the rate-determining step.[57] Lin et al. proposed that CO oxidation over Co_1/h-BN may proceed through an alternative ER mechanism (ER1) by direct formation of CO_2 from the adsorbed O_2 and CO and reduction of the metal site by gaseous CO.[65] Yang et al. proposed that CO oxidation may proceed through the formation and dissociation of an OCOAuOCO species formed by multiple preadsorbed CO and gaseous O_2 [trimolecular ER (TER)] over Au_1/h-BN.[66] A similar trimolecular ER mechanism was also proposed for Pd-based SACs.[67] Though the predicted performances of these SACs for CO oxidation were excellent according to the reported activation energies, it is still meaningful to develop tools to correlate these properties with the reaction kinetics under conditions relevant to the experiment.

Pd is regarded as the most Pt-like metal and is capable of overcoming CO poisoning through the direct pathway,[68] especially when deposited over a carbon support as the cathode material in fuel cells using formic acid[69,70] and alcohols.[70−72] Stimulated by previous works, we theoretically explored the reaction network for CO oxidation over PdGr that was recently synthesized and tested in butyldiene and acetylene hydrogenation.[49,52] We used first-principles-based thermodynamics calculations, capable of overcoming the "pressure" and "temperature" gaps, to describe the relative stability of surface species and the reaction thermodynamics. Microkinetics simulations were also performed to distinguish the dominant reaction pathway and to predict the performance under experimental relevant conditions. We expect these findings will help in rationalizing the current knowledge on the catalytic performance of SACs.

2. THEORETICAL METHODS

All first-principles-based calculations were performed using the Perdew−Burke−Ernzerhof functional within the generalized gradient approximation with the DSPP pseudopotential as implemented in DMol^3.[73−78] Transition states (TSs) were located through the synchronous method with conjugated gradient refinements and confirmed by the frequency analysis.[79,80] The population analysis was performed with the Hirshfeld scheme.[81] Within the above methods, the calculated bulk lattice parameters of Pd and graphene are 4.04 and 2.46 Å, respectively.[82,83] In the microkinetics simulations, the adsorption of gaseous molecules was treated with an early gaslike TS, and desorption of surface species was assumed to be in equilibrium with adsorption.[84−86] The rate constants of surface reactions were calculated in an Arrhenius form, as established in the TS theory according to the first-principles-based statistics and thermodynamics.[87] The apparent activation barrier at each condition was calculated by fitting the Arrhenius plots ($\ln(\text{reaction rate}/s^{-1}) \approx (1/T)$ curves).[88] The microkinetics simulations were performed by numerically solving the differential chemical master equation system based on the reaction network with MATLAB software. The steady state was determined by evaluating the evolution of surface species coverage with respect to time. Further details concerning the theoretical methods and models can be found in the Supporting Information.

https://dx.doi.org/10.1021/acscatal.9b04840
ACS Catal. 2020, 10, 3084−3093

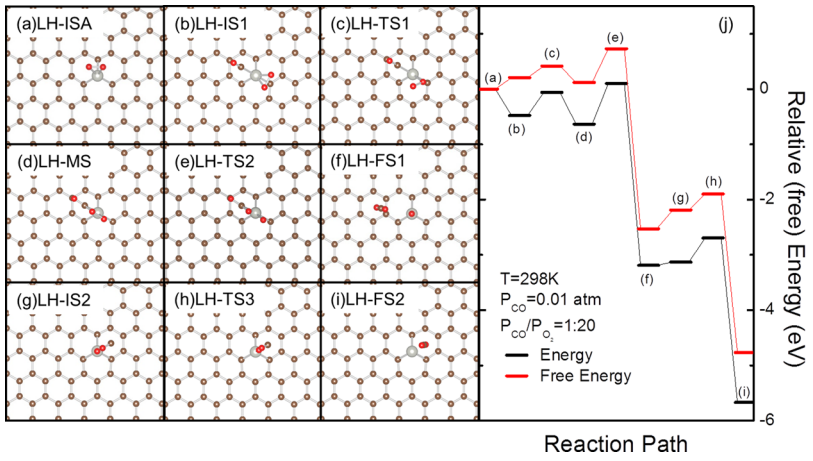

Figure 2. Optimized structures of the reaction species involved, including reaction intermediates, TSs and products (a–i), and (free) energy profiles (j) for CO oxidation over PdGr through the rLH pathway. In (a–i), the C, O, and Pd atoms are in brown, red, and silver, respectively. In (j), the bracketed letters correspond to the structures shown in (a–i). All energies are calculated with respect to LH-ISA (a).

3. RESULTS AND DISCUSSION

3.1. Thermodynamics Considerations. Our investigation started with the thermodynamics calculations to understand the stability of potential reaction species under experimental CO oxidation conditions. We calculated the formation Gibbs free energies of all potential reactants at various temperatures (T) at P_{CO}/P_{O_2} = 1:1 and P_{CO} = 0.01 atm (Figure 1, Table S1), which are conventionally used to characterize the CO oxidation performance of a catalyst.[89]

The calculation suggests that the replacement of a sp^2 C atom by a Pd atom (PdGr, Figure 1a, E_b = −5.43 eV) is thermodynamically more favorable by more than 4 eV than the adsorption of a Pd atom on pristine graphene (E_b = −1.10 eV) because of the possible interactions between Pd and the graphene monovacancy. In PdGr, the Pd−C distances are ∼1.96 Å, and Pd is calculated to be positively charged by 0.53 |e|. These findings are in good agreement with the reported X-ray photoelectron spectroscopy of Pd atoms dispersed over graphene and N-doped graphene, where the Pd atoms are confirmed to be positively charged and undercoordinated reaction centers.[49,90] According to the calculated ΔG of the potential reaction species (Figure 1, right panel), O_2 adsorbed on PdGr (Figure 1b, E_{ad} = −1.05 eV) was found to be the most plausible species at temperatures ranging between 250 and 450 K. Here, O_2 lies immediately on top of Pd, with the stretched O−O bond (1.34 Å) parallel to one pair of C atoms directly bonded to Pd, and interacts with Pd through states of t_{2g} symmetry. The Hirshfeld charge on Pd is 0.56 |e|, and the spin is mainly localized on the O atoms. Reactants, such as CO, prefer to form σ−π interactions with transition metals, and this is also valid for PdGr. The ΔG curves (Figure 1j) of CO adsorption (Figure 1c, E_{ad} = −0.83 eV) and CO + O_2 coadsorption (Figure 1d, E_{ad} = −1.53 eV) stand right above that of O_2 adsorption and are negative from 250 to 450 K and intersect each other at ∼330 K, showing that CO + O_2 may form from the O_2 adsorption structure via coadsorption or ligand exchange. As for the other coadsorption species, such as coadsorption of 2 CO, 2 O_2, 3 CO, and 2 CO + O_2 (Figure 1e–h), and other reaction species, such as the van der Waals complexes formed between adsorbed O_2 and gaseous CO (Figure 1i), and so forth, the ΔG curves are much higher in energy than those for O_2, CO, and CO + O_2 (Figure 1j). Though these species may potentially exist, their coverage would be much lower than those for O_2, CO + O_2, and CO, and they would evolve into more stable species by ligand desorption or exchange. Our results from standard first-principles-based calculations (Figure 1) and also with the consideration of van der Waals interactions (Figure S1, Supporting Information) clearly indicate that the O_2 adsorption over PdGr (Figure 1b) is the most plausible reaction species in the 250–450 K temperature range under CO oxidation conditions. We also investigated the impact of CO and O_2 chemical potential on the relative stability in terms of ΔG of these reaction species by varying the CO and O_2 partial pressure in the range of 0.01–0.2 atm in the same temperature interval (Figure S2, Supporting Information). Though the calculated values of ΔG of these identified major reactants, namely, O_2, CO, CO + O_2, and 2CO (Figure 1b–e), may shift due to the variation of reaction conditions, O_2 adsorption is still the most plausible, considering that the ΔG curves of CO and CO + O_2 remain right above that of O_2. This is in reasonable agreement with the experimental finding that the active reaction species in CO oxidation on atomically dispersed transition metal over various substrates is positively charged or even oxidized metal atoms.[12,21,22,64,91] The calculated stretching frequency of CO (Figure 1c) is slightly red-shifted from that of gaseous CO, that is, from 2143 to 2128 cm^{-1}, and further shifted to 2125 cm^{-1} in CO + O_2 (Figure 1d), confirming the positively charged nature of the atomically dispersed Pd atoms. Similar red shifts of the C═O stretching frequency have been reported for CO oxidation over Pd- and Pt-based SACs and nanoparticle catalysts.[7,9,12,21,63,64,92] As the proposed model (Figure 1a, PdGr) has provided consistent evidence for the positively charged nature of PdGr, we moved on to investigate its performance in CO oxidation.

3.2. Determination of the Reaction Network. We considered the aforementioned reaction pathways, namely, rLH, ER1, ER2, and TER, as the potential reaction pathways for CO oxidation. We focused on the pathways initiating from O_2 adsorption and referred this structure as LH-ISA (Figure 2a). We treated the other pathways, such as TER, as starting with the ligand-exchange reaction between gaseous CO and adsorbed O_2. The optimized structures and corresponding (free) energy profiles of the reaction species for the rLH pathway at 298 K are shown in Figure 2.

https://dx.doi.org/10.1021/acscatal.9b04840
ACS Catal. 2020, 10, 3084−3093

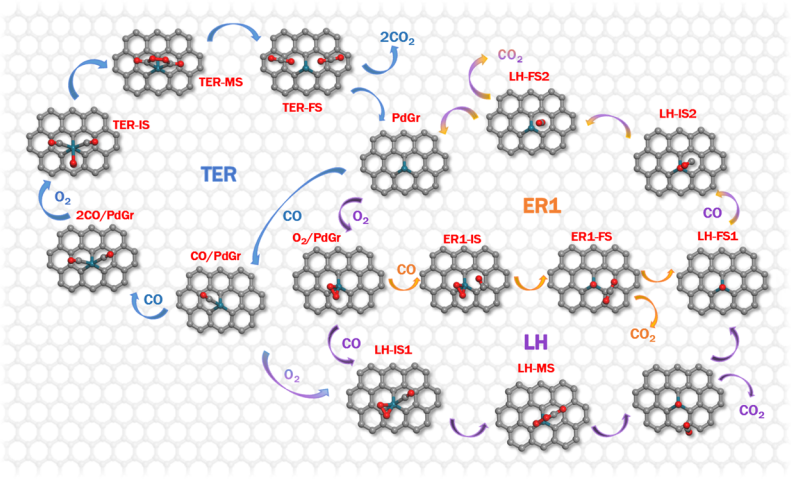

Figure 3. Reaction network for CO oxidation over PdGr. The reaction species appearing on ER1, TER, and rLH pathways are connected with dark blue, orange, and purple lines, respectively, whereas the species shared by different pathways are connected by lines of joint colors. The names of the surface species along each path are shown in red, whereas their abbreviated names in the microkinetics simulations are in light blue.

3.2.1. rLH Pathway. The rLH pathway for CO oxidation can be described as the sequence of elementary steps shown in Figure 2. As Pd in LH-ISA is not fully coordinated, CO may coadsorb with O_2 (LH-IS1, Figure 2b) with the CO in plane with one of the Pd−C bonds perpendicular to the O−O bond. According to the calculated ΔG (Figures 1 and 2j), the formation of LH-IS1 is only 0.21 eV less plausible than that of LH-ISA. The small endothermicity can be attributed to the repulsive interaction between coadsorbed CO and O_2, whereas the calculated E_{ad} of CO is −0.48 eV with respect to LH-ISA, about 0.35 eV less than E_{ad} of CO in Figure 1c. Considering the large exothermicity for the formation of LH-ISA (∼−5.5 eV), LH-IS1 may exist but with a smaller population. Further, variation of ΔG from LH-ISA to LH-IS1 also suggests that the formed species would be active for subsequent reactions.[92] Driven by the electrostatic interaction between $O(O_2)$ and C(CO) (with partial charges of 0.12 and −0.14 |e|, respectively), the C(CO) atom moves to interact with $O(O_2)$. By crossing a TS (LH-TS1, Figure 2c), where the O−C distance is decreased from 2.99 Å in LH-IS1 to 2.81 Å, a peroxide intermediate (LH-MS, Figure 2d) is formed. The calculated energy and free-energy barriers for the formation of LH-MS are 0.42 and 0.21 eV, respectively. The newly formed C−O bond stabilizes the reaction product and makes the formation of LH-MS slightly exothermic (ΔG = −0.09 eV) with respect to LH-IS1. In LH-MS, the O−O distance of 1.50 Å and the O−O stretching frequency of 811 cm^{-1} are both typical of O−O bonds in peroxides.[93] The C═O stretching frequency in LH-MS was calculated as 1754 cm^{-1}, which falls in the higher range of experimentally reported values.[12,21,64] Because of the instability of the peroxide O−O bond, LH-MS undergoes dissociation and a CO_2 molecule is formed (LH-FS1, Figure 2f) by charge reorganization within the newly formed C−O bond (LH-TS2, Figure 2e). When going from LH-MS to LH-TS2, the C═O distance retains the value of 1.22 Å, whereas the O−O and Pt−C distances elongate from 1.50 and 2.15 Å to 1.88 and 2.33 Å, respectively, and the C−O distance is shortened from 1.37 to 1.25 Å, showing the tendency for breaking the O−O bond and reorganizing the structure to form CO_2. Accompanying this structure change, charge is accumulated on C and 2 $O(O_2)$ atoms, as evidenced by the calculated increase of Hirshfeld charges on the C and 2 $O(O_2)$ atoms from 0.03, −0.08, and −0.25 |e| in LH-MS to 0.10, −0.10, and −0.30 |e|, respectively, in LH-TS2. This charge accumulation is further enhanced in LH-FS1 where the charges on C, $O(CO_2)$, O(Pt), and Pt are 0.27, −0.14, −0.48, and 0.58 |e|, respectively, implying the subsequent oxidation of Pd in this process and the weak binding of CO_2 to the Pd═O center. This is in agreement with the calculated E_{ad} of CO_2 in LH-FS1 of only −0.08 eV.

According to the rLH pathway for SACs, the subsequent reaction may proceed with the formation of the van der Waals complex between gaseous CO and O(Pt) (LH-IS2, Figure 2g). The calculated ΔE and ΔG between LH-FS1 and LH-IS2 are only 0.06 and 0.34 eV, respectively. The electrostatic interaction between positively charged C(CO) (0.05 |e|) and the 0.41|e| negatively charged O(Pt) stabilizes LH-IS2 and initiates the subsequent reaction by an induced charge transfer from 5σ, the highest occupied molecular orbital (HOMO) of CO, to π^*, the lowest unoccupied molecular orbital (LUMO) on O(Pt). CO moves toward O(Pt) in this process to reach the TS (LH-TS3, Figure 2h), where the C−O(Pt) distance decreases to 1.91 Å and the calculated Hirshfeld charge on C and O(Pt) changes to 0.04 and −0.36 |e|, respectively, indicating a charge transfer from CO to O for the formation of the C═O bond (Figure S3). By crossing the energy barrier of 0.44 eV (LH-TS3), another CO_2 is formed (LH-FS2, Figure 2i). As the calculated E_{ad} of CO_2 is only −0.08 eV, desorption of CO_2 would be easy even at room temperature.

3.2.2. Alternative Reaction Pathways. It is well accepted that CO_3 species (Figure S4) are formed according to ER types of reaction pathways. Narula et al. proposed that the CO_3 species are formed from coadsorbed CO and O_2 (LH-IS1).[21] The calculated barrier for CO_3 formation through this mechanism is at least 1.22 eV. Previously, a barrier of 1.48 eV was reported for a similar mechanism of CO oxidation over Pd/Al_2O_3 SACs.[64] As this barrier is much higher than E_{ad} of O_2 or CO, desorption would take place prior to CO_3 formation; therefore, we did not include this pathway into the reaction network. We also investigated the CO oxidation through other alternative paths, namely, the ER1 and TER pathways (Tables 1 and S2; Figures 3 and S5−S8). The conventional ER mechanism for CO oxidation over metals requires the adsorption and activation of one of the reaction species on

https://dx.doi.org/10.1021/acscatal.9b04840
ACS Catal. 2020, 10, 3084−3093

Table 1. Calculated Reaction Barriers, Rate Constants, and Coverage of Rate-Determining Reaction Species and Reaction Rate for the Rate-Determining Steps for CO Oxidation on PdGr through rLH, ER1, and TER Pathways[a]

		T = 298 K, P_{CO}/P_{O_2} = 1:20, P_{CO} = 0.01 atm			T = 325 K, P_{CO}/P_{O_2} = 1:1, P_{CO} = 0.20 atm		
reaction	barrier (eV)	k[c]	c of RDS[d]	r[e]	k[c]	c of RDS[d]	r[e]
rLH Pathway							
LH-IS1 → LH-MS	0.41						
LH-MS[b] → LH-FS1	0.72	3.20×10^{2}	8.63×10^{-5}	2.76×10^{-2}	3.13×10^{3}	3.16×10^{-4}	9.89×10^{-1}
LH-IS2 → LH-FS2	0.44						
ER1 Pathway							
ER1-IS[b] → ER1-FS	0.73	4.89×10^{1}	1.13×10^{-12}	5.55×10^{-11}	2.15×10^{2}	5.16×10^{-11}	1.11×10^{-8}
TER Pathway							
TER-IS → TER-MS	0.25						
TER-MS[b] → TER-FS	0.42	4.55×10^{6}	1.18×10^{-14}	5.36×10^{-8}	9.93×10^{6}	1.23×10^{-12}	1.22×10^{-5}

[a]The nomenclature of reaction species is the same as those in Figure 2, S5, and S6. Please note that the ER1 pathway also goes through LH-IS2, LH-TS3, and LH-FS2 after CO_2 desorption from ER1-FS. [b]The rate-determining species along each reaction path. [c]The rate constant for the rate-determining step along each reaction path. [d]The coverage of the rate-determining species at the steady state along each reaction path. [e]The reaction rate along each reaction path at the steady state.

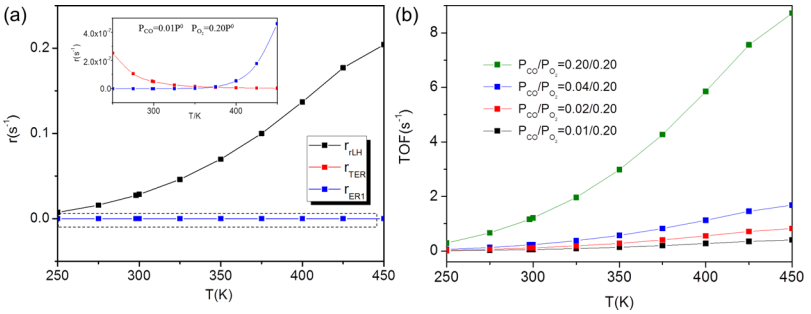

Figure 4. Variation of reaction rates with temperature at P_{CO} = 0.01 atm and P_{O_2} = 0.20 atm (a) and variation of the TOF with temperature at P_{O_2} = 0.20 atm with different P_{CO}/P_{O_2} ratios (b). As the reaction rates along the TER and ER1 pathways are similar, they are enlarged in the inset of (a).

the reaction site. Though O_2 is activated upon adsorption on PdGr, as evidenced by the elongated O−O distance (1.34 Å), dissociation of O_2 is still endothermic by 1.09 eV, with an energy barrier of 2.09 eV, implying that the adsorbed O_2 may desorb prior to dissociation. This is similar to what happens on pristine graphene where O_2 is physically adsorbed and graphene oxidation with O_2 is a spin-restricted reaction with high reaction barriers.[94] Considering the thermostability of CO + O_2 and O_2 and $2O_2$ and the small barrier for LH-MS formation (Figures 1 and 2), PdGr cannot effectively catalyze O_2 dissociation to oxidize the graphene substrate. As there is a charge transfer from PdGr to O_2 (−0.15 |e| on each O atom), the HOMO and LUMO of adsorbed O_2 are both $2\pi^*$ orbitals, whereas the HOMO and LUMO of CO are 5σ and $2\pi^*$ orbitals, respectively. For the reaction of gaseous CO with O_2 adsorbed on PdGr to form CO_3 species through the ER2 pathway, only the interaction between CO $2\pi^*$ and O_2 $2\pi^*$ is symmetry allowed, which results in the unusual charge transfer from O_2 to CO. We confirmed this charge transfer by calculating the charge-density difference for the CO_3 formation from CO and adsorbed O_2 (Figure S4, Supporting Information). To continue the reaction process along this path, O_2 has to dissociate into O atoms before the reaction with CO through an endothermic process of 2.09 eV. This is why the calculated reaction barrier along the ER2 pathway is much higher than for the other pathways and is quite similar to that for O_2 dissociation. Therefore, CO oxidation along the ER2 pathway[57] was not considered in the reaction network. We noticed that the interaction between CO 5σ and O_2 $2\pi^*$ orbitals is slightly plausible when the O−O(O_2)−C(CO) angle is about 130°; but in this case, the reaction may proceed along the ER1 or the rLH pathway.[65]

3.3. Insights from Microkinetics Modeling and First-Principles Data. A continuous flow reactor was built, and a series of microkinetics simulations were performed based on the aforementioned results from first-principles-based calculations and the TS theory (Figure 3, Tables S2−S5) to distinguish the dominant reaction pathway and the rate-determining steps under experimental conditions. The TSs of the highest barrier on the ER1, TER, and rLH pathways are the direct attack of gaseous CO to O_2 (ER1-IS to ER1-FS, Figure 3), the dissociation of the OCOOCO intermediate (TER-MS to TER-FS, Figure 3), and the dissociation of the peroxide intermediate (LH-MS to LH-FS1, Figure 3), respectively (Tables 1 and S3−S5).

The rates calculated at different reaction conditions (T, P_{CO}, and P_{O_2}) for the three reaction pathways suggest that the rLH one is dominant over 250−450 K, and high turn over frequencies (TOFs) are possible for CO oxidation over PdGr (Table 1 and Figure 4). The TER pathway is preferred over the ER1 one, though their contributions to the overall reaction rate and TOF are at least 10^6 smaller in magnitude than that of the rLH pathway. A close look at the evolution of the surface species coverage at T = 298.15 K, P_{CO} = 0.01 atm, and P_{CO}/P_{O_2} = 1:20 (Figure S9a) shows that O_2 adsorption (LH-ISA) dominates the population of the surface species at the steady state, whereas the peroxide species (LH-MS) ranks second and

https://dx.doi.org/10.1021/acscatal.9b04840
ACS Catal. 2020, 10, 3084−3093

the CO + O_2 coadsorption structure (LH-IS1) ranks third. This is in excellent agreement with the thermodynamics analysis according to which LH-ISA is the most plausible surface species in the temperature range from 200 to 450 K. The high population of LH-MS can be attributed to the large dissociation barrier to form CO_2 and adsorbed O on Pd. On the other hand, the high population of LH-IS1 is due to its intrinsic thermostability as shown in Figure 1 and its crucial position on the reaction pathways for formation of other surface species (Figure 3). As the reaction proceeds, the adsorbed atomic oxygen and bare PdGr (Figure 1a) are also minor species on the surface. This is due to the fact that after the dissociation of LH-MS, the adsorbed atomic oxygen may quickly react with CO through a reaction barrier of only 0.44 eV. In this sense, the relatively poor coverage of LH-IS2 is not only due to its low thermostability but also due to the fast reactions involved. All surface species with significant coverage belong to the rLH pathway. As for the other pathways, such as ER1 and TER, although the reaction rate constants of the rate-limiting steps (i.e., the dissociation of the OCOOCO intermediate for TER and the direct reduction of adsorbed O_2 by CO for ER1) are much larger or similar to that for the rLH pathway, the 10^6 lower coverage of the corresponding surface species makes the contribution of these pathways to the total reaction rate and TOF negligible (Table 1, Figure 4a). To back up these findings, we also performed simulations under the same reaction condition, starting with bare PdGr and PdGr fully covered with CO (Figure S9b,c). Though starting with different surface species, both the reactors reached the same steady state according to the final coverage of the reaction species. However, the detailed evolution processes on PdGr are different according to the variation of surface coverage at the beginning of the reaction. This suggests that there is no potential CO or O_2 poisoning taking place over PdGr because of the high preference for O_2 adsorption and, correlatively, relatively weak CO adsorption. When exposed to gaseous mixtures under reaction conditions, O_2 adsorption may take place to compete with CO adsorption through the formation of a coadsorption structure or by ligand exchange or desorption.

We note that the CO oxidation rate through the rLH pathway is sensitive to and increases with the reaction temperature. As LH-MS is the rate-determining species and its dissociation is the rate-determining step on the rLH pathway, the variation of free energy of LH-MS and LH-TS2 and the free-energy barrier for dissociation of LH-MS were calculated (Figure S10). Obviously, ΔG of LH-MS is slightly more sensitive and increases faster with temperature than that of LH-TS2. This can be attributed to the instability of its peroxide O−O bond that makes the free-energy barrier decrease with the reaction temperature and partially contributes to the increase of the reaction rate.

The TOFs at different P_{CO} values were also calculated (Figure 4b). As CO cannot compete with O_2 for adsorption on PdGr, the increase of P_{CO} helps to increase the surface coverage of LH-IS1 and leads to a high coverage of LH-MS that directly impacts the total reaction rate and the TOF. Specifically, an increase of P_{CO} from 0.01 to 0.02 atm at 298 K with P_{O_2} fixed at 0.20 atm may lead to an increase of TOF from 0.05 to 0.11 s^{-1}. This effect, together with the positive effect of a temperature increase due to the intrinsic instability of the peroxide, makes the TOF and reaction rate drastically increase with P_{CO} and temperature. An increase of the P_{CO}/P_{O_2} ratio to 1:1 and temperature from 298 to 325 K may lead to a nearly 40-fold increase of the TOF from 0.05 to 1.98 s^{-1}. We also performed the apparent barrier analysis under these two conditions by fitting the Arrhenius plot, and the calculated apparent barriers are 15.4 and 15.6 kJ/mol, respectively (Table S6 and Figure S11). In this sense, the catalytic performance of PdGr would be comparable with some of the reported SACs for CO oxidation, such as Pt/m-Al_2O_3 (0.18 s^{-1} at 525 K)[9] and Pt/θ-Al_2O_3 (0.19 s^{-1} at 525 K).[64] Because we did not include the formation and impact of the carbonate species into the reaction network, we possibly underestimate the overall catalytic performance of PdGr, considering the experimentally justified promotion effect of carbonate in CO oxidation at low temperatures.[11,12]

The C═O stretching frequency was widely used to investigate the mechanism of CO oxidation. However, because of the strong light absorbance of graphene, there is less data for diffuse reflectance Fourier transform (DRIFT) or in situ infrared (IR) during CO oxidation over SACs or metal nanoparticles supported on graphene. We tried to connect the calculated results with the available DRIFT and in situ IR data for CO oxidation over Pt/Pd SACs. The calculated C═O stretching frequency in LH-MS is 1754 cm^{-1}. Previously, C═O stretching of 1700−1800 cm^{-1} was observed during CO oxidation on CoO_x/Al_2O_3, Pt/CeO_2, and Pt/Al_2O_3 and was assigned to the C═O stretching frequency of species formed with lattice oxygen or in aldehyde-related function groups during CO oxidation.[11,12,64,95,96] The present calculated value is reasonable considering the coordination environment of the lattice oxygen. For comparison, the C═O stretching frequency in the carbonate CO_3 species potentially formed on PdGr (Figure S3, Supporting Information) was calculated to be 1584 cm^{-1}, in excellent agreement with previous suggestions that the CO stretching frequency in the 1500−1700 cm^{-1} range corresponds to the carbonate species. However, another recent investigation based on the in situ vibrational spectrum showed that there is potentially more than one kind of CO_3 intermediate formed during CO oxidation over the Pt/Al_2O_3 SAC according to the observed broad vibration band from 1500−1730 cm^{-1}. The detailed analysis showed that the C═O stretching at 1670 cm^{-1} corresponds to a reactive "CO_3" intermediate that cannot be assigned to conventional carbonate on the Al_2O_3 substrate and accounts for the reaction kinetics for CO_2 evolution. The one observed at ∼1610 cm^{-1} can be attributed to the carbonates formed on Pt or Al_2O_3.[12] Though the C═O stretching frequency is dependent on the metal−support interaction and the exact form of the metal species, the calculated C═O stretching frequencies for peroxide and carbonate species show a similar trend, and the calculated C═O stretching frequencies of the carbonate species are usually lower than those of the unstable peroxides. In this sense, we proposed that the peroxide species may behave in the same way as the observed reactive "CO_3" species over PdGr.

Additional electronic structure arguments can further corroborate and validate the predicted catalytic performance of PdGr (Figure 5). We note that the Pd atom binds nearly equally with the C atoms around the vacancy on graphene (Figure 1a), and their interactions induce a strong charge transfer (Figure 5, inset). The graphene defect states are down-shifted to overlap with the Pd-sp and Pd-d states below the

https://dx.doi.org/10.1021/acscatal.9b04840
ACS Catal. 2020, 10, 3084−3093

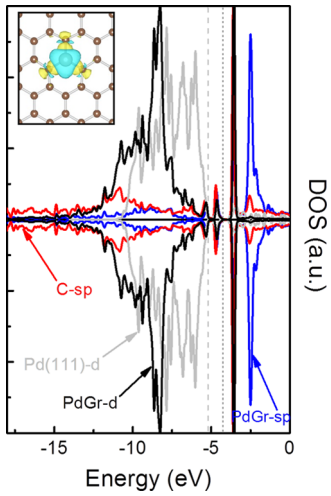

Figure 5. Projected density of states for PdGr and contour plot of charge density difference (inset). In the inset, the contour value is 1×10^{-6} a.u., and the charge accumulation and depletion regions are in yellow and light blue, respectively. The C and Pd atoms are in brown and silver, respectively. The zero of the energy scale is the vacuum level. Fermi levels (E_F) of PdGr and Pd(111) are marked with black and light gray dashed lines, respectively.

Fermi level (E_F). Some Pd states are up-shifted by about 1 eV to resonate with the C-sp states. This hybridization between Pd and graphene defect makes the calculated E_F of PdGr higher than that of Pd(111), and the calculated work functions of PdGr and Pd(111) slabs are 4.27 and 5.20 eV, respectively.[97−99] The lowered work function suggests that PdGr may exhibit different affinity for CO and O_2 as well as for other reaction species, compared with conventional transition metals (Figure 1, Table S1), and accounts for the thermostability of the reaction species on the rLH pathway. As the occupied frontier states of PdGr are mainly composed of Pd-sp and C-sp (Figure 5), the charge transfer to bind O_2 is more favored than $\sigma-\pi$ coordination with CO. This is consistent with the thermodynamic analysis and microkinetics simulation results that O_2 adsorption is thermodynamically preferred over CO adsorption (Table 1 and Figure 1) and explains the anti-CO-poisoning feature of PdGr and the relatively superior stability of the surface species on the rLH pathway. In this sense, the superior catalytic performance of PdGr in CO oxidation can be attributed to the specific electronic structure of PdGr.

4. CONCLUSIONS

To connect the experimental observations with the theoretical predictions on catalytic performance over graphene-supported SACs, we investigated the thermodynamics and kinetics of CO oxidation over PdGr. Combining first-principles-based thermodynamics calculations and microkinetics modeling, we showed that a positively charged PdGr with sp-type frontier states can exhibit a rather high low-temperature activity for CO oxidation. Under reaction conditions, O_2 binds strongly with Pd acting as the major surface species to convert CO. We also showed that the microkinetics simulation is an effective tool to distinguish the dominant reaction pathways. CO oxidation over PdGr mainly proceeds with the rLH pathway, with the dissociation of the peroxide species as the rate-limiting step. The reaction rate is strongly dependent on the thermostability of the reaction species. The reaction rates along some previously proposed pathways with even lower activation energy are significantly slower as compared with the rLH pathway because of the low surface coverage of the involved species originating from their poor thermostability. In conclusion, the predicted catalytic performance of PdGr can be attributed to the specific electronic structure of PdGr originating from the Pd−C interactions, with positively charged Pd exposing sp-type frontier states. We expect that these findings would help to understand the performance of SACs and rationalize the design and fabrication of SACs with superior catalytic performance.

■ ASSOCIATED CONTENT

Supporting Information

The Supporting Information is available free of charge at https://pubs.acs.org/doi/10.1021/acscatal.9b04840.

Supplementary detailed theoretical methods used for the first-principles-based calculations and microkinetics simulations, energy and the most plausible structure for the potential reaction species, free-energy curves for the most plausible reaction species at different partial pressures of CO and O_2 with and without consideration of the van der Waals interactions, structure and charge-density difference plots for LH-TS3 and CO_3 species, atomic structures and corresponding free-energy curves for CO oxidation through the TER and ER1 pathways, energy and free energy profile for CO oxidation over PdGr, evolution of coverage of surface reaction species over PdGr in a continuous flow reactor starting with O_2 fully covered, bare, and CO fully covered PdGr at 298 K, P_{CO} = 0.01 atm, and P_{O_2} = 0.20 atm, calculated reaction rates and rate constants at 298 K, P_{CO} = 0.01 atm, and P_{O_2} = 0.20 atm and 325 K, P_{CO} = 0.20 atm, and P_{O_2} = 0.20 atm, calculated overall reaction rates and Arrhenius plots for calculation of the apparent reaction barriers and the variation of the free energy of LH-MS, and LH-TS2 and free-energy barrier for LH-MS dissociation with temperature (PDF)

■ AUTHOR INFORMATION

Corresponding Authors

Xin Liu − *State Key Laboratory of Fine Chemicals, Department of Chemistry, Dalian University of Technology, Dalian 116024, P. R. China*; orcid.org/0000-0002-4422-4108; Email: xliu@dlut.edu.cn

Yu Han − *KAUST Catalysis Center (KCC), King Abdullah University of Science and Technology, Thuwal 23955-6900, Saudi Arabia*; orcid.org/0000-0003-1462-1118; Email: yu.han@kaust.edu.sa

Changgong Meng − *State Key Laboratory of Fine Chemicals, Department of Chemistry, Dalian University of Technology, Dalian 116024, P. R. China*; orcid.org/0000-0003-1662-0565; Email: cgmeng@dlut.edu.cn

Authors

Meng Xu − *State Key Laboratory of Fine Chemicals, Department of Chemistry, Dalian University of Technology, Dalian 116024, P. R. China*

Lingyun Wan − *State Key Laboratory of Fine Chemicals, Department of Chemistry, Dalian University of Technology, Dalian 116024, P. R. China*

https://dx.doi.org/10.1021/acscatal.9b04840
ACS Catal. 2020, 10, 3084−3093

Hongdan Zhu − *State Key Laboratory of Fine Chemicals, Department of Chemistry, Dalian University of Technology, Dalian 116024, P. R. China*
Kexin Yao − *Multi-Scale Porous Materials Center, Institute of Advanced Interdisciplinary Studies, School of Chemistry and Chemical Engineering, Chongqing University, Chongqing 400044, P. R. China*
Roberto Linguerri − *Université Gustave Eiffel, COSYS/LISIS Laboratory, Marne-la-Vallée F-77454, France*
Gilberte Chambaud − *Université Gustave Eiffel, COSYS/LISIS Laboratory, Marne-la-Vallée F-77454, France;* orcid.org/0000-0002-8031-2746

Complete contact information is available at: https://pubs.acs.org/10.1021/acscatal.9b04840

Author Contributions

X.L. conceived the research and wrote the manuscript. M.X performed the calculations and analyzed the results with the help of L.W. and H.Z. M.X. is responsible for all calculation results disclosed. X.L., Y.H., and C.M. provided the materials and tools. Y.H., R.L., C.M., G.C., and K.Y. commented on the results and proofed the manuscript. X.L. finalized the manuscript. All authors have given approval to the final version of the manuscript.

Notes

The authors declare no competing financial interest.

■ ACKNOWLEDGMENTS

This work was supported by NSFC (21771029, 11811530631, 21573034, 21373036, and 21103015). X.L. also acknowledges the support from the Chinese Scholarship Council (201706060254), the Special Academic Partner GCR Program from King Abdullah University of Science and Technology (KAUST), and the EU-2020 Advanced Project (grant agreement no. 670173). The supercomputer time was supported by the High Performance Computing Center at the Dalian University of Technology, National Supercomputing Center in Guangzhou, China and the Supercomputing Center at KAUST.

■ REFERENCES

(1) Korotkikh, O.; Farrauto, R. Selective catalytic oxidation of CO in H-2: Fuel cell applications. *Catal. Today* **2000**, *62*, 249−254.
(2) Bion, N.; Epron, F.; Moreno, M.; Mariño, F.; Duprez, D. Preferential Oxidation of Carbon Monoxide in the Presence of Hydrogen (PROX) over Noble Metals and Transition Metal Oxides: Advantages and Drawbacks. *Top. Catal.* **2008**, *51*, 76−88.
(3) Park, E. D.; Lee, D.; Lee, H. C. Recent progress in selective CO removal in a H-2-rich stream. *Catal. Today* **2009**, *139*, 280−290.
(4) Liu, K.; Wang, A.; Zhang, T. Recent Advances in Preferential Oxidation of CO Reaction over Platinum Group Metal Catalysts. *ACS Catal.* **2012**, *2*, 1165−1178.
(5) Kašpar, J.; Fornasiero, P.; Hickey, N. Automotive catalytic converters: current status and some perspectives. *Catal. Today* **2003**, *77*, 419−449.
(6) Fiore, A. M.; Naik, V.; Spracklen, D. V.; Steiner, A.; Unger, N.; Prather, M.; Bergmann, D.; Cameron-Smith, P. J.; Cionni, I.; Collins, W. J.; Dalsøren, S.; Eyring, V.; Folberth, G. A.; Ginoux, P.; Horowitz, L. W.; Josse, B.; Lamarque, J.-F.; MacKenzie, I. A.; Nagashima, T.; O'Connor, F. M.; Righi, M.; Rumbold, S. T.; Shindell, D. T.; Skeie, R. B.; Sudo, K.; Szopa, S.; Takemura, T.; Zeng, G. Global air quality and climate. *Chem. Soc. Rev.* **2012**, *41*, 6663−6683.
(7) Ding, K.; Gulec, A.; Johnson, A. M.; Schweitzer, N. M.; Stucky, G. D.; Marks, L. D.; Stair, P. C. Identification of active sites in CO oxidation and water-gas shift over supported Pt catalysts. *Science* **2015**, *350*, 189−192.
(8) DeRita, L.; Resasco, J.; Dai, S.; Boubnov, A.; Thang, H. V.; Hoffman, A. S.; Ro, I.; Graham, G. W.; Bare, S. R.; Pacchioni, G.; Pan, X.; Christopher, P. Structural evolution of atomically dispersed Pt catalysts dictates reactivity. *Nat. Mater.* **2019**, *18*, 746.
(9) Zhang, Z.; Zhu, Y. H.; Asakura, H.; Zhang, B.; Zhang, J. G.; Zhou, M. X.; Han, Y.; Tanaka, T.; Wang, A. Q.; Zhang, T.; Yan, N. Thermally stable single atom Pt/m-Al2O3 for selective hydrogenation and CO oxidation. *Nat. Commun.* **2017**, *8*, 16100.
(10) Wang, H.; Liu, J.-X.; Allard, L. F.; Lee, S.; Liu, J.; Li, H.; Wang, J.; Wang, J.; Oh, S. H.; Li, W.; Flytzani-Stephanopoulos, M.; Shen, M.; Goldsmith, B. R.; Yang, M. Surpassing the single-atom catalytic activity limit through paired Pt-O-Pt ensemble built from isolated Pt1 atoms. *Nat. Commun.* **2019**, *10*, 3808.
(11) Newton, M. A.; Ferri, D.; Smolentsev, G.; Marchionni, V.; Nachtegaal, M. Room-temperature carbon monoxide oxidation by oxygen over Pt/Al2O3 mediated by reactive platinum carbonates. *Nat. Commun.* **2015**, *6*, 8675.
(12) Newton, M. A.; Ferri, D.; Smolentsev, G.; Marchionni, V.; Nachtegaal, M. Kinetic Studies of the Pt Carbonate-Mediated, Room-Temperature Oxidation of Carbon Monoxide by Oxygen over Pt/Al2O3 Using Combined, Time-Resolved XAFS, DRIFTS, and Mass Spectrometry. *J. Am. Chem. Soc.* **2016**, *138*, 13930−13940.
(13) Liu, Q.; Zhang, Z. Platinum single-atom catalysts: a comparative review towards effective characterization. *Catal. Sci. Technol.* **2019**, *9*, 4821−4834.
(14) Qiao, B.; Wang, A.; Yang, X.; Allard, L. F.; Jiang, Z.; Cui, Y.; Liu, J.; Li, J.; Zhang, T. Single-atom catalysis of CO oxidation using Pt-1/FeOx. *Nat. Chem.* **2011**, *3*, 634−641.
(15) Lang, R.; Xi, W.; Liu, J. C.; Cui, Y. T.; Li, T. B.; Lee, A. F.; Chen, F.; Chen, Y.; Li, L.; Li, L.; Lin, J.; Miao, S.; Liu, X. Y.; Wang, A. Q.; Wang, X. D.; Luo, J.; Qiao, B. T.; Li, J.; Zhang, T. Non defect-stabilized thermally stable single-atom catalyst. *Nat. Commun.* **2019**, *10*, 234.
(16) Shan, S.; Petkov, V.; Yang, L.; Luo, J.; Joseph, P.; Mayzel, D.; Prasai, B.; Wang, L.; Engelhard, M.; Zhong, C.-J. Atomic-Structural Synergy for Catalytic CO Oxidation over Palladium−Nickel Nanoalloys. *J. Am. Chem. Soc.* **2014**, *136*, 7140−7151.
(17) Li, J.; Guan, Q.; Wu, H.; Liu, W.; Lin, Y.; Sun, Z.; Ye, X.; Zheng, X.; Pan, H.; Zhu, J.; Chen, S.; Zhang, W.; Wei, S.; Lu, J. Highly Active and Stable Metal Single-Atom Catalysts Achieved by Strong Electronic Metal-Support Interactions. *J. Am. Chem. Soc.* **2019**, *141*, 14515−14519.
(18) Kropp, T.; Lu, Z.; Li, Z.; Chin, Y.-H. C.; Mavrikakis, M. Anionic Single-Atom Catalysts for CO Oxidation: Support-Independent Activity at Low Temperatures. *ACS Catal.* **2019**, *9*, 1595−1604.
(19) Alexopoulos, K.; Wang, Y.; Vlachos, D. G. First-Principles Kinetic and Spectroscopic Insights into Single-Atom Catalysis. *ACS Catal.* **2019**, *9*, 5002−5010.
(20) Peterson, E. J.; Delariva, A. T.; Lin, S.; Johnson, R. S.; Guo, H.; Miller, J. T.; Kwak, J. H.; Peden, C. H. F.; Kiefer, B.; Allard, L. F.; Ribeiro, F. H.; Datye, A. K. Low-temperature carbon monoxide oxidation catalysed by regenerable atomically dispersed palladium on alumina. *Nat. Commun.* **2014**, *5*, 4885.
(21) Narula, C. K.; Allard, L. F.; Wu, Z. L. Ab Initio Density Functional Calculations and Infra-Red Study of CO Interaction with Pd Atoms on theta-Al2O3 (010) Surface. *Sci. Rep.* **2017**, *7*, 6231.
(22) Yang, T.; Fukuda, R.; Hosokawa, S.; Tanaka, T.; Sakaki, S.; Ehara, M. A Theoretical Investigation on CO Oxidation by Single-Atom Catalysts M-1/-Al2O3 (M=Pd, Fe, Co, and Ni). *ChemCatChem* **2017**, *9*, 1222−1229.
(23) Abbet, S.; Heiz, U.; Häkkinen, H.; Landman, U. CO oxidation on a single Pd atom supported on magnesia. *Phys. Rev. Lett.* **2001**, *86*, 5950−5953.
(24) Hülsey, M. J.; Zhang, B.; Ma, Z.; Asakura, H.; Do, D. A.; Chen, W.; Tanaka, T.; Zhang, P.; Wu, Z.; Yan, N. In situ spectroscopy-

guided engineering of rhodium single-atom catalysts for CO oxidation. *Nat. Commun.* **2019**, *10*, 1330.
(25) Zhang, L.; Filot, I. A. W.; Su, Y.-Q.; Liu, J.-X.; Hensen, E. J. M. Understanding the Impact of Defects on Catalytic CO Oxidation of LaFeO3-Supported Rh, Pd, and Pt Single-Atom Catalysts. *J. Phys. Chem. C* **2019**, *123*, 7290−7298.
(26) Kimble, M. L.; Castleman, A. W.; Mitrić, R.; Bürgel, C.; Bonačić-Koutecký, V. Reactivity of atomic gold anions toward oxygen and the oxidation of CO: Experiment and theory. *J. Am. Chem. Soc.* **2004**, *126*, 2526−2535.
(27) Yang, M.; Allard, L. F.; Flytzani-Stephanopoulos, M. Atomically Dispersed Au−(OH)x Species Bound on Titania Catalyze the Low-Temperature Water-Gas Shift Reaction. *J. Am. Chem. Soc.* **2013**, *135*, 3768−3771.
(28) Liu, J.-C.; Wang, Y.-G.; Li, J. Toward Rational Design of Oxide-Supported Single-Atom Catalysts: Atomic Dispersion of Gold on Ceria. *J. Am. Chem. Soc.* **2017**, *139*, 6190−6199.
(29) Qiao, B.; Liang, J.-X.; Wang, A.; Xu, C.-Q.; Li, J.; Zhang, T.; Liu, J. J. Ultrastable single-atom gold catalysts with strong covalent metal-support interaction (CMSI). *Nano Res.* **2015**, *8*, 2913−2924.
(30) Lu, Y.; Wang, J.; Yu, L.; Kovarik, L.; Zhang, X.; Hoffman, A. S.; Gallo, A.; Bare, S. R.; Sokaras, D.; Kroll, T.; Dagle, V.; Xin, H.; Karim, A. M. Identification of the active complex for CO oxidation over single-atom Ir-on-MgAl2O4 catalysts. *Nat. Catal.* **2019**, *2*, 149−156.
(31) Lin, J.; Qiao, B.; Liu, J.; Huang, Y.; Wang, A.; Li, L.; Zhang, W.; Allard, L. F.; Wang, X.; Zhang, T. Design of a Highly Active Ir/Fe(OH)x Catalyst: Versatile Application of Pt-Group Metals for the Preferential Oxidation of Carbon Monoxide. *Angew. Chem., Int. Ed.* **2012**, *51*, 2920−2924.
(32) Oh, S.; Hoflund, G. Low-temperature catalytic carbon monoxide oxidation over hydrous and anhydrous palladium oxide powders. *J. Catal.* **2007**, *245*, 35−44.
(33) Fu, Q.; Li, W.-X.; Yao, Y.; Liu, H.; Su, H.-Y.; Ma, D.; Gu, X.-K.; Chen, L.; Wang, Z.; Zhang, H.; Wang, B.; Bao, X. Interface-Confined Ferrous Centers for Catalytic Oxidation. *Science* **2010**, *328*, 1141−1144.
(34) Qiao, B.; Wang, A.; Yang, X.; Allard, L. F.; Jiang, Z.; Cui, Y.; Liu, J.; Li, J.; Zhang, T. Single-atom catalysis of CO oxidation using Pt(1)/FeO(x). *Nat. Chem.* **2011**, *3*, 634−641.
(35) Liu, J. Catalysis by Supported Single Metal Atoms. *ACS Catal.* **2017**, *7*, 34−59.
(36) Wang, A.; Li, J.; Zhang, T. Heterogeneous single-atom catalysis. *Nat. Rev. Chem.* **2018**, *2*, 65−81.
(37) Yang, X.-F.; Wang, A.; Qiao, B.; Li, J.; Liu, J.; Zhang, T. Single-Atom Catalysts: A New Frontier in Heterogeneous Catalysis. *Acc. Chem. Res.* **2013**, *46*, 1740−1748.
(38) Krasheninnikov, A. V.; Lehtinen, P. O.; Foster, A. S.; Pyykko, P.; Nieminen, R. M. Embedding Transition-Metal Atoms in Graphene: Structure, Bonding, and Magnetism. *Phys. Rev. Lett.* **2009**, *102*, 126807.
(39) Bayatsarmadi, B.; Zheng, Y.; Vasileff, A.; Qiao, S. Z. Recent Advances in Atomic Metal Doping of Carbon-based Nanomaterials for Energy Conversion. *Small* **2017**, *13*, 1700191.
(40) Tang, Q.; Zhou, Z.; Chen, Z. Graphene-related nanomaterials: tuning properties by functionalization. *Nanoscale* **2013**, *5*, 4541−4583.
(41) Wang, H.; Wang, Q.; Cheng, Y.; Li, K.; Yao, Y.; Zhang, Q.; Dong, C.; Wang, P.; Schwingenschlögl, U.; Yang, W.; Zhang, X. X. Doping Monolayer Graphene with Single Atom Substitutions. *Nano Lett.* **2011**, *12*, 141−144.
(42) Xi, J.; Sun, H.; Wang, D.; Zhang, Z.; Duan, X.; Xiao, J.; Xiao, F.; Liu, L.; Wang, S. Confined-interface-directed synthesis of Palladium single-atom catalysts on graphene/amorphous carbon. *Appl. Catal., B* **2018**, *225*, 291−297.
(43) Chen, X.; Yu, L.; Wang, S.; Deng, D.; Bao, X. Highly active and stable single iron site confined in graphene nanosheets for oxygen reduction reaction. *Nano Energy* **2017**, *32*, 353−358.
(44) Zhang, L.; Jia, Y.; Gao, G.; Yan, X.; Chen, N.; Chen, J.; Soo, M. T.; Wood, B.; Yang, D.; Du, A.; Yao, X. Graphene Defects Trap Atomic Ni Species for Hydrogen and Oxygen Evolution Reactions. *Chem* **2018**, *4*, 285−297.
(45) Cui, X.; Ren, P.; Deng, D.; Deng, J.; Bao, X. Single layer graphene encapsulating non-precious metals as high-performance electrocatalysts for water oxidation. *Energy Environ. Sci.* **2016**, *9*, 123−129.
(46) Xi, J.; Sun, H.; Wang, D.; Zhang, Z.; Duan, X.; Xiao, J.; Xiao, F.; Liu, L.; Wang, S. Confined-interface-directed synthesis of Palladium single-atom catalysts on graphene/amorphous carbon. *Appl. Catal., B* **2018**, *225*, 291−297.
(47) Huang, X.; Xia, Y.; Cao, Y.; Zheng, X.; Pan, H.; Zhu, J.; Ma, C.; Wang, H.; Li, J.; You, R.; Wei, S.; Huang, W.; Lu, J. Enhancing both selectivity and coking-resistance of a single-atom Pd-1/C3N4 catalyst for acetylene hydrogenation. *Nano Res.* **2017**, *10*, 1302−1312.
(48) Feng, Y.; Zhou, L.; Wan, Q.; Lin, S.; Guo, H. Selective hydrogenation of 1,3-butadiene catalyzed by a single Pd atom anchored on graphene: the importance of dynamics. *Chem. Sci.* **2018**, *9*, 5890−5896.
(49) Yan, H.; Cheng, H.; Yi, H.; Lin, Y.; Yao, T.; Wang, C.; Li, J.; Wei, S.; Lu, J. Single-Atom Pd-1/Graphene Catalyst Achieved by Atomic Layer Deposition: Remarkable Performance in Selective Hydrogenation of 1,3-Butadiene. *J. Am. Chem. Soc.* **2015**, *137*, 10484−10487.
(50) Huang, F.; Deng, Y.; Chen, Y.; Cai, X.; Peng, M.; Jia, Z.; Xie, J.; Xiao, D.; Wen, X.; Wang, N.; Jiang, Z.; Liu, H.; Ma, D. Anchoring Cu1 species over nanodiamond-graphene for semi-hydrogenation of acetylene. *Nat. Commun.* **2019**, *10*, 4431.
(51) Zhang, J.; Deng, Y.; Cai, X.; Chen, Y.; Peng, M.; Jia, Z.; Jiang, Z.; Ren, P.; Yao, S.; Xie, J.; Xiao, D.; Wen, X.; Wang, N.; Liu, H.; Ma, D. Tin-Assisted Fully Exposed Platinum Clusters Stabilized on Defect-Rich Graphene for Dehydrogenation Reaction. *ACS Catal.* **2019**, *9*, 5998−6005.
(52) Huang, F.; Deng, Y.; Chen, Y.; Cai, X.; Peng, M.; Jia, Z.; Ren, P.; Xiao, D.; Wen, X.; Wang, N.; Liu, H.; Ma, D. Atomically Dispersed Pd on Nanodiamond/Graphene Hybrid for Selective Hydrogenation of Acetylene. *J. Am. Chem. Soc.* **2018**, *140*, 13142−13146.
(53) Deng, D.; Chen, X.; Yu, L.; Wu, X.; Liu, Q.; Liu, Y.; Yang, H.; Tian, H.; Hu, Y.; Du, P.; Si, R.; Wang, J.; Cui, X.; Li, H.; Xiao, J.; Xu, T.; Deng, J.; Yang, F.; Duchesne, P. N.; Zhang, P.; Zhou, J.; Sun, L.; Li, J.; Pan, X.; Bao, X. A single iron site confined in a graphene matrix for the catalytic oxidation of benzene at room temperature. *Sci. Adv.* **2015**, *1*, No. e1500462.
(54) Liu, X.; Yang, Y.; Chu, M.; Duan, T.; Meng, C.; Han, Y. Defect Stabilized Gold Atoms on Graphene as Potential Catalysts for Ethylene Epoxidation: A First-principles Investigation. *Catal. Sci. Technol.* **2016**, *6*, 1632−1641.
(55) Pulido, A.; Boronat, M.; Corma, A. Propene Epoxidation with H-2/H2O/O-2 Mixtures Over Gold Atoms Supported on Defective Graphene: A Theoretical Study. *J. Phys. Chem. C* **2012**, *116*, 19355−19362.
(56) Lu, Y.-H.; Zhou, M.; Zhang, C.; Feng, Y.-P. Metal-Embedded Graphene: A Possible Catalyst with High Activity. *J. Phys. Chem. C* **2009**, *113*, 20156−20160.
(57) Li, Y.; Zhou, Z.; Yu, G.; Chen, W.; Chen, Z. CO Catalytic Oxidation on Iron-Embedded Graphene: Computational Quest for Low-Cost Nanocatalysts. *J. Phys. Chem. C* **2010**, *114*, 6250−6254.
(58) Song, E. H.; Wen, Z.; Jiang, Q. CO Catalytic Oxidation on Copper-Embedded Graphene. *J. Phys. Chem. C* **2011**, *115*, 3678−3683.
(59) Liu, X.; Sui, Y.; Duan, T.; Meng, C.; Han, Y. CO oxidation catalyzed by Pt-embedded graphene: a first-principles investigation. *Phys. Chem. Chem. Phys.* **2014**, *16*, 23584−23593.
(60) Langmuir, I. The mechanism of the catalytic action of platinum in the reactions 2CO + O2= 2CO2 and 2H2+ O2= 2H2O. *Trans. Faraday Soc.* **1922**, *17*, 621−654.
(61) Duan, Z.; Henkelman, G. CO Oxidation on the Pd(111) Surface. *ACS Catal.* **2014**, *4*, 3435−3443.

https://dx.doi.org/10.1021/acscatal.9b04840
ACS Catal. 2020, 10, 3084−3093

(62) Piccinin, S.; Stamatakis, M. CO Oxidation on Pd(111): A First-Principles-Based Kinetic Monte Carlo Study. *ACS Catal.* **2014**, *4*, 2143−2152.
(63) Allian, A. D.; Takanabe, K.; Fujdala, K. L.; Hao, X.; Truex, T. J.; Cai, J.; Buda, C.; Neurock, M.; Iglesia, E. Chemisorption of CO and Mechanism of CO Oxidation on Supported Platinum Nanoclusters. *J. Am. Chem. Soc.* **2011**, *133*, 4498−4517.
(64) Moses-DeBusk, M.; Yoon, M.; Allard, L. F.; Mullins, D. R.; Wu, Z.; Yang, X.; Veith, G.; Stocks, G. M.; Narula, C. K. CO Oxidation on Supported Single Pt Atoms: Experimental and ab Initio Density Functional Studies of CO Interaction with Pt Atom on θ-Al2O3(010) Surface. *J. Am. Chem. Soc.* **2013**, *135*, 12634−12645.
(65) Lin, S.; Ye, X.; Johnson, R. S.; Guo, H. First-Principles Investigations of Metal (Cu, Ag, Au, Pt, Rh, Pd, Fe, Co, and Ir) Doped Hexagonal Boron Nitride Nanosheets: Stability and Catalysis of CO Oxidation. *J. Phys. Chem. C* **2013**, *117*, 17319−17326.
(66) Mao, K.; Li, L.; Zhang, W. H.; Pei, Y.; Zeng, X. C.; Wu, X. J.; Yang, J. L. A Theoretical Study of Single-Atom Catalysis of CO Oxidation Using Au Embedded 2D h-BN Monolayer: A CO-Promoted O-2 Activation. *Sci. Rep.* **2015**, *4*, 5441.
(67) Xu, G.; Wang, R.; Yang, F.; Ma, D.; Yang, Z.; Lu, Z. CO oxidation on single Pd atom embedded defect-graphene via a new termolecular Eley-Rideal mechanism. *Carbon* **2017**, *118*, 35−42.
(68) Arenz, M.; Stamenkovic, V.; Schmidt, T. J.; Wandelt, K.; Ross, P. N.; Markovic, N. M. The electro-oxidation of formic acid on Pt-Pd single crystal bimetallic surfaces. *Phys. Chem. Chem. Phys.* **2003**, *5*, 4242−4251.
(69) Yang, J.; Tian, C.; Wang, L.; Fu, H. An effective strategy for small-sized and highly-dispersed palladium nanoparticles supported on graphene with excellent performance for formic acid oxidation. *J. Mater. Chem.* **2011**, *21*, 3384−3390.
(70) Chen, X.; Wu, G.; Chen, J.; Chen, X.; Xie, Z.; Wang, X. Synthesis of "Clean" and Well-Dispersive Pd Nanoparticles with Excellent Electrocatalytic Property on Graphene Oxide. *J. Am. Chem. Soc.* **2011**, *133*, 3693−3695.
(71) Xu, C.; Wang, X.; Zhu, J. Graphene-Metal Particle Nanocomposites. *J. Phys. Chem. C* **2008**, *112*, 19841−19845.
(72) Gotoh, K.; Kawabata, K.; Fujii, E.; Morishige, K.; Kinumoto, T.; Miyazaki, Y.; Ishida, H. The use of graphite oxide to produce mesoporous carbon supporting Pt, Ru, or Pd nanoparticles. *Carbon* **2009**, *47*, 2120−2124.
(73) Delley, B. An all-Electron numerical-method for solving the local density functional for polyatomic-molecules. *J. Chem. Phys.* **1990**, *92*, 508−517.
(74) Delley, B. From molecules to solids with the DMol(3) approach. *J. Chem. Phys.* **2000**, *113*, 7756−7764.
(75) Perdew, J. P.; Burke, K.; Ernzerhof, M. Generalized gradient approximation made simple. *Phys. Rev. Lett.* **1996**, *77*, 3865−3868.
(76) Delley, B. Hardness conserving semilocal pseudopotentials. *Phys. Rev. B: Condens. Matter Mater. Phys.* **2002**, *66*, 155125.
(77) Rappoport, D.; Crawford, N. R. M.; Furche, F.; Burke, K. Approximate Density Functionals: Which Should I Choose?. *Encyclopedia of Inorganic Chemistry*; John Wiley & Sons, Ltd., 2006; pp 1−14.
(78) Inada, Y.; Orita, H. Efficiency of numerical basis sets for predicting the binding energies of hydrogen bonded complexes: Evidence of small basis set superposition error compared to Gaussian basis sets. *J. Comput. Chem.* **2008**, *29*, 225−232.
(79) Govind, N.; Petersen, M.; Fitzgerald, G.; King-Smith, D.; Andzelm, J. A generalized synchronous transit method for transition state location. *Comput. Mater. Sci.* **2003**, *28*, 250−258.
(80) Monkhorst, H. J.; Pack, J. D. Special points for Brillouin-zone integrations. *Phys. Rev. B: Condens. Matter Mater. Phys.* **1976**, *13*, 5188−5192.
(81) Hirshfeld, F. L. Bonded-atom fragments for describing molecular charge-densities. *Theor. Chim. Acta* **1977**, *44*, 129−138.
(82) Gajdo, M.; Eichler, A.; Hafner, J. CO adsorption on close-packed transition and noble metal surfaces: trends from ab initio calculations. *J. Phys.: Condens. Matter* **2004**, *16*, 1141−1164.
(83) Castro Neto, A. H.; Guinea, F.; Peres, N. M. R.; Novoselov, K. S.; Geim, A. K. The electronic properties of graphene. *Rev. Mod. Phys.* **2009**, *81*, 109−162.
(84) Stamatakis, M.; Vlachos, D. G. A graph-theoretical kinetic Monte Carlo framework for on-lattice chemical kinetics. *J. Chem. Phys.* **2011**, *134*, 214115.
(85) Reuter, K. Ab Initio Thermodynamics and First-Principles Microkinetics for Surface Catalysis. *Catal. Lett.* **2016**, *146*, 541−563.
(86) Su, Y.-Q.; Wang, Y.; Liu, J.-X.; Filot, I. A. W.; Alexopoulos, K.; Zhang, L.; Muravev, V.; Zijlstra, B.; Vlachos, D. G.; Hensen, E. J. M. Theoretical Approach To Predict the Stability of Supported Single-Atom Catalysts. *ACS Catal.* **2019**, *9*, 3289−3297.
(87) Eyring, H. The Activated Complex in Chemical Reactions. *J. Chem. Phys.* **1935**, *3*, 107−115.
(88) Mao, Z.; Campbell, C. T. Apparent Activation Energies in Complex Reaction Mechanisms: A Simple Relationship via Degrees of Rate Control. *ACS Catal.* **2019**, *9*, 9465−9473.
(89) Wang, C.; Gu, X.-K.; Yan, H.; Lin, Y.; Li, J.; Liu, D.; Li, W.-X.; Lu, J. Water-Mediated Mars-Van Krevelen Mechanism for CO Oxidation on Ceria-Supported Single-Atom Pt-1 Catalyst. *ACS Catal.* **2017**, *7*, 887−891.
(90) Zhou, S.; Shang, L.; Zhao, Y. X.; Shi, R.; Waterhouse, G. I. N.; Huang, Y. C.; Zheng, L. R.; Zhang, T. R. Pd Single-Atom Catalysts on Nitrogen-Doped Graphene for the Highly Selective Photothermal Hydrogenation of Acetylene to Ethylene. *Adv. Mater.* **2019**, *31*, 1900509.
(91) Narula, C. K.; Stocks, G. M. Ab Initio Density Functional Calculations of Adsorption of Transition Metal Atoms on θ-Al2O3(010) Surface. *J. Phys. Chem. C* **2012**, *116*, 5628−5636.
(92) Ammal, S. C.; Heyden, A. Water-Gas Shift Activity of Atomically Dispersed Cationic Platinum versus Metallic Platinum Clusters on Titania Supports. *ACS Catal.* **2017**, *7*, 301−309.
(93) Kopecky, K. R.; Gomez, R. R. O-O Stretching Frequencies of Cyclic Peroxides - Stabilization of Peroxides by Alkoxy Substituents. *Can. J. Chem.* **1984**, *62*, 277−279.
(94) Bagsican, F. R.; Winchester, A.; Ghosh, S.; Zhang, X.; Ma, L. L.; Wang, M. J.; Murakami, H.; Talapatra, S.; Vajtai, R.; Ajayan, P. M.; Kono, J.; Tonouchi, M.; Kawayama, I. Adsorption energy of oxygen molecules on graphene and two-dimensional tungsten disulfide. *Sci. Rep.* **2017**, *7*, 1774.
(95) Zhang, Q.; Mo, S.; Li, J.; Sun, Y.; Zhang, M.; Chen, P.; Fu, M.; Wu, J.; Chen, L.; Ye, D. In situ DRIFT spectroscopy insights into the reaction mechanism of CO and toluene co-oxidation over Pt-based catalysts. *Catal. Sci. Technol.* **2019**, *9*, 4538−4551.
(96) Wang, C.-B.; Tang, C.-W.; Tsai, H.-C.; Kuo, M.-C.; Chien, S.-H. In situ FT-IR spectroscopic studies on the mechanism of the catalytic oxidation of carbon monoxide over supported cobalt catalysts. *Catal. Lett.* **2006**, *107*, 31−37.
(97) Demuth, J. E. Chemisorption of C2H2 on Pd(111) and Pt(111) - Formation of a thermally activated olefinic surface complex. *Chem. Phys. Lett.* **1977**, *45*, 12−17.
(98) Methfessel, M.; Hennig, D.; Scheffler, M. Trends of the surface relaxations, surface energies, and work-functions of the 4D transition-metals. *Phys. Rev. B: Condens. Matter Mater. Phys.* **1992**, *46*, 4816−4829.
(99) Nieuwenhuys, B. E.; Bouwman, R.; Sachtler, W. M. H. Changes in work function of group-IB and group-VIII metals on Xenon adsorption, determined by field electron and photoelectron emission. *Thin Solid Films* **1974**, *21*, 51−58.

https://dx.doi.org/10.1021/acscatal.9b04840
ACS Catal. 2020, 10, 3084−3093